Intrinsic and extrinsic electrical and thermal transport of bulk black phosphorus

Sile Hu,[1,2] Junsen Xiang,[1,3] Meng Lv,[1,2] Jiahao Zhang,[1,2] Hengcan Zhao,[1,2] Chunhong Li,[1] Genfu Chen,[1] Wenhong Wang,[1] and Peijie Sun[1]

[1]*Beijing National Laboratory for Condensed Matter Physics, Institute of Physics, Chinese Academy of Sciences, Beijing 100190, China*
[2]*University of Chinese Academy of Sciences, Beijing 100049, China*
[3]*Department of Physics, Key Laboratory of Micro-Nano Measurement-Manipulation and Physics (Ministry of Education), Beihang University, Beijing 100191, China*

(Received 14 July 2017; revised manuscript received 11 January 2018; published 26 January 2018)

We report a comprehensive investigation of the electrical, thermal, and thermoelectric transport properties of bulk single-crystalline black phosphorus in wide temperature (2–300 K) and field (0–9 T) ranges. Electrical transport below $T \approx 250$ K is found to be dominated by extrinsic hole-type charge carriers with large mobility exceeding 10^4 cm^2/V s at low temperatures. While thermal transport measurements reveal an enhanced in-plane thermal conductivity maximum $\kappa = 180$ W/m K at $T \approx 25$ K, it appears still to be largely constrained by extrinsic phonon scattering processes, e.g., the electron-phonon process, in addition to intrinsic umklapp scattering. The thermoelectric power and Nernst effect seem to be strongly influenced by ambipolar transport of charge carriers with opposite signs in at least the high-temperature region above 200 K, which diminishes the thermoelectric power factor of this material. Our results provide a timely update to the transport properties of bulk black phosphorus for future fundamental and applied research.

DOI: 10.1103/PhysRevB.97.045209

I. INTRODUCTION

Black phosphorus (BP) is a layer-structured, high-mobility semiconductor of great current interest from both fundamental and applied points of view [1]. Single- or few-layer BP is also known as phosphorene [2] and mimics the crystallographic characteristics of two-dimensional graphene, which is a few-layer form of graphite [3]. Different from graphene, which has no band gap, BP has a direct band gap E_g that can be tuned from 0.3 to 2.0 eV by scaling down the layer thickness from bulk to monolayer [2,4–6]. Tunability of E_g due to interlayer coupling yields rich possibilities for this material for future applications in nanoelectronic and optoelectronic devices.

Excellent transport properties such as high charge mobility and high thermal conductivity, although anisotropic along different in-plane directions and not as high as in graphene, are theoretically expected for few-layer BP (Refs. [6–8]). Along this line, many investigations have been devoted to BP-based nanoscaled materials and devices. The experimentally obtained quantities, e.g., charge mobility, however, mostly deviate from theoretical anticipation significantly. Specifically, while a charge mobility of $\sim 10^4$ cm^2/V s is expected for a BP monolayer at $T = 300$ K, the experimentally observed values are generally one order of magnitude smaller [9,10]. Compared to nanoscaled BP, most recent interest in bulk BP has been focused on the emerging topological phase [11,12] and superconductivity [13] under high pressure. The current knowledge on transport properties of bulk BP, in particular thermal transport, largely relies on old literature with measurements performed in limited temperature and field ranges [14].

BP crystallizes in the orthorhombic lattice with space group *cmca* consisting of layers of covalently bonded, more specifically, sp^3-hybridized, phosphorus atoms that are puckered along the c axis [Fig. 1(a)]. Similar to graphene, weak van der Waals bonding acts across the basal plane, allowing thin layers to be easily exfoliated from the bulk. The layered structure, as well as the narrow direct band gap ($E_g = 0.3$–0.5 eV at the Z point for the bulk [5,6]), makes BP attractive for another application for thermoelectrics [15,16]. The value of E_g is comparable to that of state-of-the-art thermoelectric materials like Bi_2Te_3 ($E_g \approx 0.15$ eV), and the layered structure has strong similarities to that of the superior thermoelectric material SnSe [17]. Furthermore, from a theoretical point of view, the anisotropy of in-plane electrical/thermal transport may lead to an enhanced possibility of direction-selected thermoelectric performance [18]. An in-depth experimental investigation of thermoelectric properties of bulk BP is still unavailable [19,20].

In this work, we provide a comprehensive investigation of the thermal, electrical, and thermoelectric properties of bulk single-crystalline BP. It is found that the electrical transport is dominated by extrinsic charge carriers in a wide temperature range at $T < 250$ K. Significant ambipolar transport of charge carriers with opposite signs appears to manifest in the thermoelectric power, Nernst effect, and Hall resistivity. A large in-plane thermal conductivity amounting to $\kappa = 180$ W/m K at $T \approx 25$ K was observed, indicating a long phonon mean free path exceeding 1 μm at low temperatures. This value is, however, still significantly smaller than the thickness of the sample employed, ~ 100 μm, hinting at an even higher intrinsic thermal conductivity.

II. EXPERIMENT

Bulk single-crystalline BP was prepared from red phosphorous at high pressure ($P = 2$ GPa) and high temperature

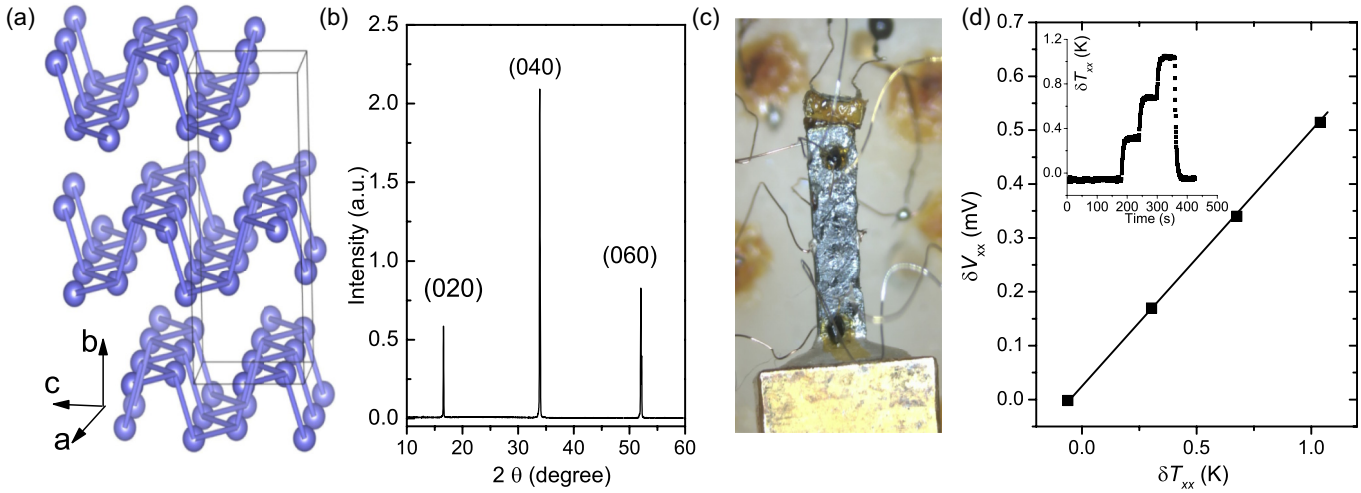

FIG. 1. (a) The layered crystal structure of black phosphorus, where the coordinate b denotes the through-plane direction, in agreement with most recent literature on this material. The in-plane a and c axes are frequently expressed as "zigzag" and "armchair" directions, respectively. (b) X-ray diffraction scan of the layer plane of IP1, where only the $(0n0)$ peaks were observed. IP2 shows practically identical results. (c) Optical image of the sample holder employed in our thermal transport measurements, with a BP sample mounted onto the cold finger. A 2.2 kΩ chip resistor was used as the heater. (d) Thermoelectric voltage δV_{xx} as a function of temperature gradient δT_{xx} recorded in one measurement run at $T = 200$ K. The value of S_{xx} was estimated by mapping the slope. Similarly, the values of S_{xy} and κ can be obtained from δV_{xy} and δP vs δT_{xx}, respectively. Inset: Illustration of the multistep heating process in the thermal transport measurement.

($T = 1000\,^{\circ}$C). For thin samples exfoliated from the bulk, the high purity and crystallinity were verified with various techniques, including x-ray diffraction and transmission electron microscope [20,21]. In-plane [i.e., the ac plane; see Fig. 1(a)] transport measurements were performed using as-exfoliated thin samples, with a typical sample dimension of approximately $0.1 \times 1 \times 4$ mm^3. We failed to accurately determine the in-plane crystallographic orientation and measured two samples (IP1 and IP2) that differed by a 90° in-plane angle. One reason for the failure is that, while the exfoliated samples are well crystallized [see the x-ray diffraction pattern in Fig. 1(b)], the as-grown bulk sample as a whole is not along the through-plane direction. Specifically, stacking up of the in-plane layers along the b axis can be easily interrupted by atomic dislocation; then the layers tilt or screw, hindering crystallographic orientation using the bulk sample. For through-plane (TP) measurements, a relatively thicker sample was used, with dimensions of $0.4 \times 1 \times 4$ mm^3. As noted above, the through-plane sample may include considerable crystallographic defects.

The electrical resistivity ρ_{xx} and Hall resistivity ρ_{xy} were measured using a physical properties measurement system (Quantum Design) from room temperature (RT) down to $T = 2$ K in magnetic fields up to $B = 9$ T. For thermal conductivity κ, thermoelectric power S_{xx}, and Nernst effect S_{xy} measurements, a homemade setup utilizing a conventional steady-state heat-flow technique was employed [see Fig. 1(c)]. The thin sample was mounted onto a copper-made cold finger on one side, with the other side suspended and attached to a chip resistor (2.2 kΩ), which was used as a heater. The magnetic field was always applied perpendicular to the layer plane for in-plane samples and perpendicular to the b axis for the through-plane sample. The temperature gradient δT built along the sample was detected by a thin ($\phi = 25\,\mu$m) $AuFe_{0.07\%}$-chromel thermocouple, which was calibrated in the magnetic field. The heater and thermocouple are supported by thin nylon wires, and all lead wires on the holder adopt $\phi = 25\,\mu$m manganin to reduce thermal loss.

Prior to each measurement process, thermal equilibrium has to be critically checked. Then, multiple heating steps were applied to the sample consecutively [see Fig. 1(d)]. The number of heating steps and their duration can be changed in order to optimize the measurement. From the slopes of the corresponding thermoelectric voltages δV_{xx}, δV_{xy} and the heating power δP vs δT_{xx}, one obtains the values of S_{xx}, S_{xy}, and κ, respectively. The typical δT_{xx} was set to 0.5% T. The longitudinal contributions to S_{xy} and ρ_{xy} are field even and can be eliminated by reversing the direction of the magnetic field. Finally, we note that the conventional steady-state thermal measurement technique is fundamentally different from the noncontact, transient techniques frequently employed in recent thermal transport studies of BP. For example, the so-called beam-offset method is a kind of pump-probe measurement, where the surface heating of a material via laser pulses is monitored by a time-delayed sensing beam [22–24]. There, the thermal penetration depth that depends on the modulation frequency of the pump beam may have a considerable effect on thermal conductance.

III. EXPERIMENTAL RESULTS AND ANALYSIS

A. Electrical resistivity and Hall effect

Electrical transport of bulk single-crystalline BP was investigated in the 1980s following the successful growth of a large single crystal under pressure [25] and was rediscovered recently in terms of magnetic-field [21] and pressure dependences [10,12]. Figure 2 shows the in-plane and through-plane $\rho_{xx}(T)$ measured in various transverse magnetic fields. Upon cooling from RT down to $T = 2$ K, $\rho_{xx}(T)$ increases by nearly four orders of magnitude for all samples, in agreement with

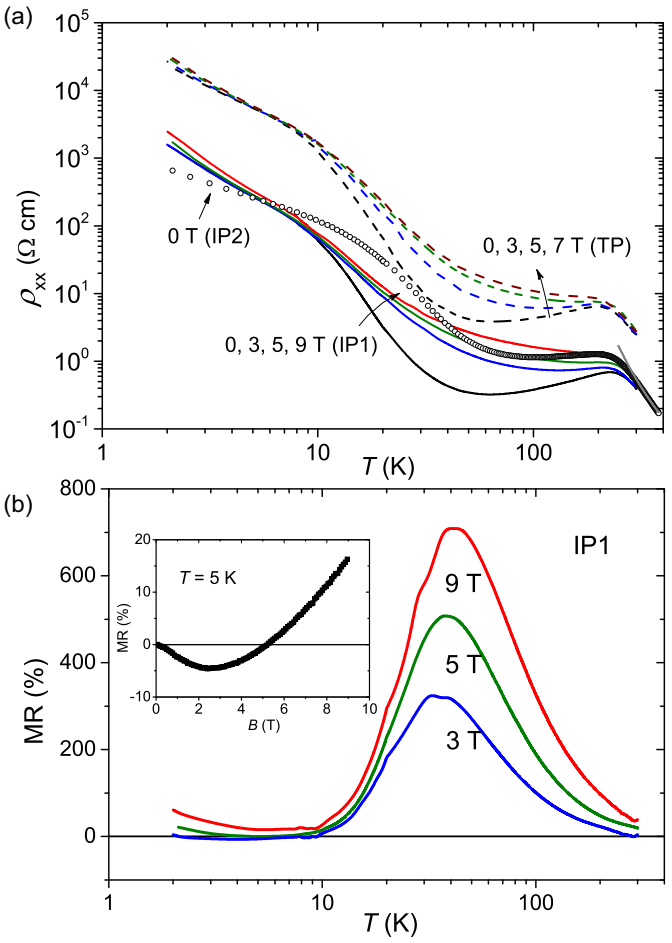

FIG. 2. (a) Electrical resistivity $\rho_{xx}(T)$ of the in-plane (IP1 and IP2) and the through-plane (TP) samples measured in different magnetic fields. The gray line on top of the high-T $\rho_{xx}(T)$ of sample IP2 illustrates a thermally activated behavior with $E_g \approx 0.288$ eV. (b) Magnetoresistance (MR) $= [\rho_{xx}(B) - \rho_{xx}(0T)]/\rho_{xx}(0T)$ measured as a function of temperature in different magnetic fields for sample IP1. The inset shows the isothermal MR(B) at $T = 5$ K.

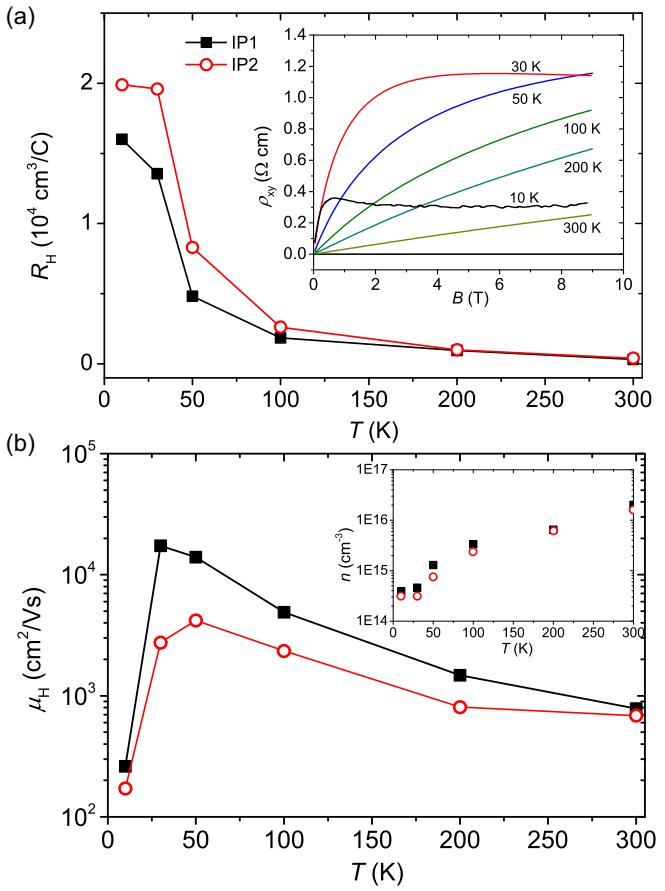

FIG. 3. (a) Initial Hall coefficient R_H estimated for the two in-plane samples as a function of temperature. Inset: Isothermal Hall resistivity $\rho_{xy}(B)$ of sample IP1. (b) Hall mobility μ_H ($= R_H/\rho_{xx}$) versus temperature for the same samples. Inset: Carrier concentration n estimated as $1/eR_H$.

previous reports [10,21,25–27]. While the temperature profiles of the in-plane and through-plane resistivity are qualitatively the same, their values differ by nearly one order of magnitude. Moreover, $\rho_{xx}(T)$ of the in-plane sample IP2 is larger than that of IP1 over the whole temperature range, indicating that the crystallographic direction of the former (latter) sample is close to the a (c) axis, given the previously known electrical anisotropy [25].

The nonmonotonic variation of $\rho_{xx}(T)$ below RT depicts the importance of extrinsic charge carriers in the current BP samples. Only at $T > 300$ K does $\rho_{xx}(T)$ follow the thermally activated function $\rho_{xx}(T) \propto \exp(E_g/2k_BT)$, with $E_g \approx 0.288$ eV estimated for IP2 [see Fig. 2(a)]. The value of E_g is in agreement with the previous estimate based on transport measurements [25,28] as well as the theoretically calculated direct gap (Ref. [6]), indicating intrinsic semiconducting transport above RT. The intermediate region (70 K $< T <$ 250 K) is characterized by a positive temperature coefficient of resistivity, i.e., $d\rho/dT > 0$, which results from extrinsic charge carriers scattered by phonons. In the low-T region ($T <$ 50 K), $\rho_{xx}(T)$ recovers an exponential increase upon cooling due to the reduced number of charge carriers thermally activated from the impurity level. A weak saturation tendency towards zero temperature was confirmed at $T <$ 10 K, which marks the temperature range where Anderson localization with hopping conduction [26,29] had been proposed. The magnetoresistance (MR) as a function of temperature, shown in Fig. 2 (b), has an enhanced maximum between $T =$ 30 and 50 K, where Hall mobility assumes its peak [see Fig. 3(b)]. By contrast, weak negative MR at low temperatures ($T <$ 10 K) and low fields ($B <$ 5 T) can be confirmed [Fig. 2(b), inset], consistent with the weak localization of charge carriers as proposed for this range. By applying a small magnetic field, the quantum interference characterizing the wave function of the weak-localization state is destroyed, leading to reduced electrical resistivity, i.e., a negative MR.

The Hall coefficient $R_H(T)$, estimated from the initial slope of the Hall resistivity $\rho_{xy}(B)$ [Fig. 3(a), inset], is shown in the main panel of Fig. 3(a) for IP1 and IP2. The value of $R_H(T)$ is positive in the whole temperature range investigated, reflecting a p-type conductance, as has usually been observed for pristine BP single crystals [25,30]. The apparent Hall number $n = 1/eR_H$ is rather low, on the order of 10^{15} cm^{-3} in

the extrinsic regime [see Fig. 3(b), inset], which is comparable to a previous report [25]. The Hall mobility $\mu_H(T)$ [Fig. 3(b)] amounts to nearly 10^3 cm^2/V s at RT and further increases upon cooling, up to $\mu_H > 1 \times 10^4$ cm^2/V s at $T = 30$ K for sample IP1. Such a high carrier mobility in bulk BP has already been known for decades [25]. A comparison of $n(T)$ and $\mu_H(T)$ between samples IP1 and IP2 implies that the lower mobility is the leading reason for the higher resistivity of the latter sample (see Fig. 2). On the other hand, the Hall mobility $\mu_H(T)$ reported for few-layer BP is generally one order of magnitude smaller, limited by the impurities at the interface with the substrate. An exceptionally large μ_H of 6000 cm^2/V s was realized only recently in a van der Waals heterostructure of few-layer BP [9].

The nonlinearity of the Hall resistivity $\rho_{xy}(B)$ [Fig. 3(a), inset] deserves further attention. It is believed to be intimately related to the field-dependent thermoelectric properties that will be discussed below. Similar behavior of $\rho_{xy}(B)$ has already appeared in previous reports [21,27]. While the nonlinearity of $\rho_{xy}(B)$ is able to be quantitatively fitted by a two-carrier model, the fitting parameters employed can be very different. Either an electron-hole [21] or a hole-hole [27] two-carrier model can explain these data. One apparent reason of such uncertainty lies in the strongly anisotropic electrical transport within the basal plane. This invalidates the assumption of isotropic conductivity (e.g., $\rho_{xx} = \rho_{yy}$) that is generally employed during data analysis [21,27]. As will be discussed below, a two-carrier transport with activated holes and electrons appears to be more likely because of (i) the temperature-dependent thermoelectric properties at high temperatures $T > 200$ K and (ii) the isothermal $S_{xx}(B)$, which decreases with field at all temperatures between 10 K and RT, despite the corresponding MR(B) being positive. Typical ambipolar conduction of different types of carriers has also been reported for BP under various gate voltages [4].

B. Thermal conductivity

The thermal conductivity of BP is another transport property that is attracting much attention [7,18,22–24,31–33]. This attention is reminiscent of the research interest in the thermal transport of graphene and related carbon-based materials, to which a tremendous number of efforts have been devoted (see Ref. [34] for a review). While for thermoelectric application a low value of κ is desired in order to reduce heat loss, in order for BP to be integrated into microelectronic devices, a high value of κ is technically beneficial. Therefore, a reliable assessment of the intrinsic thermal conductivity of BP, i.e., the heat conduction limited by anharmonic phonon dynamics, appears to be of critical importance.

First-principles calculations based on density functional theory predict anisotropic thermal conductivities for bulk BP with $\kappa_a = 102$ (zigzag), $\kappa_b = 6.5$ (through plane), and $\kappa_c = 39$ W/m K (armchair) at RT, respectively [22,23]. This large anisotropy in κ originates from the anisotropic group velocity of the acoustic phonons, as well as anisotropic phonon relaxation times along different principal axes [7,16,22,23]. The latter is a consequence of anisotropic umklapp processes. Unlike for the electrical properties, experimental investigations of thermal conductivity of bulk and few-layer BP were generally confined only to RT due to the limitation of thermal-transport experiment techniques. The reported values at RT reveal great scattering with $\kappa_a = 15$–101 W/m K, $\kappa_b = 3$–7.3 W/m K, and $\kappa_c = 5$–36 W/m K (Refs. [20,22–24]) for the bulk (see Table I) and even smaller and scattered values for nanoscaled devices [31,32]. A relatively comprehensive investigation of anisotropic thermal conductivity over an extended temperature range (80–300 K) was conducted recently, in which $\kappa(T)$ of bulk BP flakes was measured by the noncontact pump-probe technique [23].

Figure 4(a) shows $\kappa(T)$ of the three BP samples measured between RT and $T = 2$ K using the conventional steady-state technique. The electronic contribution κ_e to the measured values of κ can be estimated from the Wiedemann-Franz law, $\kappa_e \rho_{xx}/T = L_0$ based on the measured values of $\rho_{xx}(T)$, where the Lorenz number $L_0 \equiv \frac{\pi^2}{3}(\frac{k_B}{2})^2 = 2.44 \times 10^{-8}$ W Ω K^{-2}. κ_e estimated in this way is less than 0.1% in the whole temperature range (for example, $\kappa_e \approx 2 \times 10^{-3}$ W/m K at RT, where $\rho_{xx} \approx 0.4$ Ω cm) and is therefore neglected throughout our discussion. All $\kappa(T)$ curves have an enhanced maximum at low temperature characteristic of the phononic contribution to a crystalline solid. However, the enhancement of κ with decreasing temperature deviates from the T^{-1} dependence that is anticipated when heat-carrying phonons are solely scattered by intrinsic umklapp processes. The maximum of

TABLE I. Experimental values of room-temperature thermal conductivity (in W/m K) for bulk BP in the literature. The temperature range of the measurement and sample thickness are shown as well. The maximum κ along the most thermally conductive a axis, if available, is given in a footnote.

κ_a	κ_b	κ_c	T range (K)	Thickness	Reference
62–86	3.5–4.5	26–34	300	138–652 nm	[24]
84–101	4.3–5.5	26–36	300	30–50 μm	[22]
12–27		5–15	30–350	60–310 nm[a]	[32]
73–93	5.7–7.3	23–33	80–300	100–300 μm[b]	[23]
20–40		10–20	300	9–30 nm	[31]
∼15	∼3	∼10	10–300	2 mm[c]	[20]
			3–300	200 μm[d]	

[a] $\kappa_a(T)$ assumes a maximum of 40 W/m K at $T \approx 100$ K.
[b] $\kappa_a(T)$ increases up to 360 W/m K at 80 K, the lowest temperature of the measurements.
[c] $\kappa_a(T)$ assumes a maximum of 34 W/m K at $T \approx 70$ K.
[d] Polycrystalline sample. $\kappa \approx 15$ W/m K at RT, and the maximum $\kappa(T)$ amounts to ∼50 W/m K at 35 K.

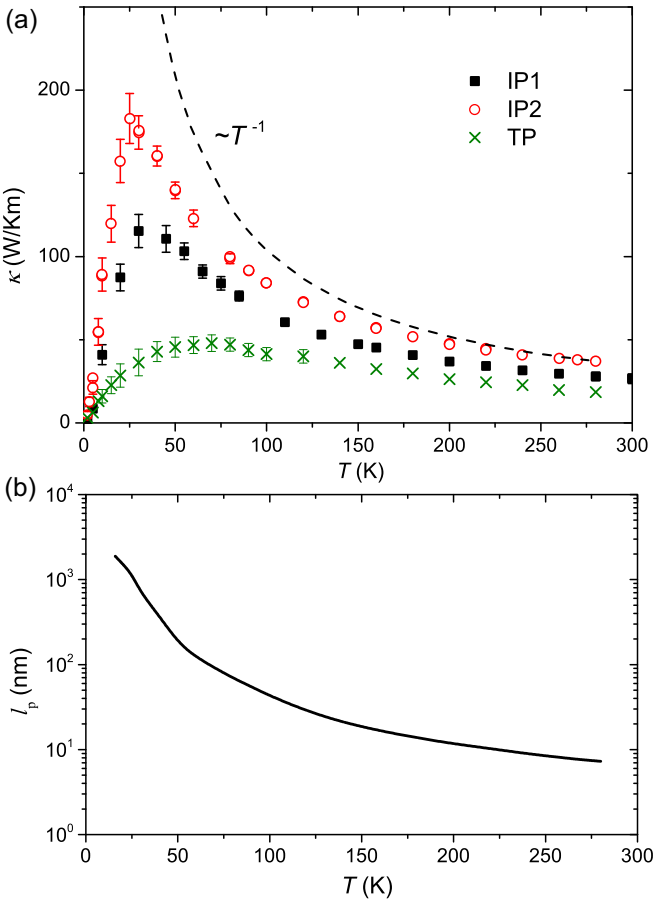

FIG. 4. (a) Thermal conductivity κ as a function of temperature for the samples IP1, IP2, and TP. A T^{-1}-dependent line characteristic of intrinsic thermal conductivity of umklapp processes is also indicated for comparison. (b) Phonon mean-free path l_p estimated from the kinetic formula as a function of temperature for sample IP2, i.e., the more thermally conductive sample. Note that this estimation serves only as a rough estimate of l_p, which in reality is phonon mode dependent [23].

$\kappa(T)$ amounts to 180 (IP2) and 120 W/m K (IP1) at $T \approx 25$ K. By contrast, $\kappa(T)$ of the sample TP assumes a broad maximum of 50 W/m K at $T \approx 70$ K. The values of $\kappa(T)$ at RT are 28, 37, and 18 W/m K for IP1, IP2, and TP, respectively. Noticeably, the observed values of κ are smaller for the in-plane samples but larger for the through-plane sample than theoretical prediction. In other words, our measurements yield more isotropic values of $\kappa(T)$. Previous thermal measurements with much thicker samples have revealed a similar temperature dependence but much smaller values for all directions [20] (see also Table I). The larger κ values for IP2 are consistent with our conjecture based on anisotropic resistivity that the closer the crystallographic orientation of this sample is to the a (zigzag) axis, the more thermally conductive the axis expected theoretically is [22,23].

The $\kappa(T)$ along the a axis reported by Sun *et al.* [23] amounts to 360 W/m K at $T = 80$ K, i.e., the lowest temperature of their measurements, and decreases following T^{-1} upon increasing temperature. This is, to our knowledge, the largest thermal conductivity so far experimentally obtained for BP. The smaller in-plane $\kappa(T)$ values in our measurements are partially ascribable to the random crystallographic orientation of the sample employed. In addition, the deviation from T^{-1} dependence shown in Fig. 4(a) suggests other fundamental mechanisms that, in addition to umklapp processes, limit phonon propagation. For example, a small number of extrinsic charge carriers (less than $10^{17}/\text{cm}^{-3}$) may greatly reduce the intrinsic thermal conductivity of a semiconductor by electron-phonon coupling, as has been observed in silicon [35]. The much weaker anisotropy [in particular that of the in-plane and through-plane samples; see Fig. 4(a)] is likely due to the characteristics of the conventional thermal measurement technique in measuring very anisotropic materials, as well as the crystalline imperfections in the through-plane sample as discussed in Sec. II. Different from the noncontact optical techniques [22–24] which probe the phonon dynamics locally (spot radius $\sim 1\,\mu$m) and estimate the anisotropic thermal conductivity components through an analytical way, in a conventional thermal-transport measurement, the thermal diffusion is long range, sensitive to any misalignment and various defects of the sample used. In particular, due to the dislocation of BP layers anticipated for the through-plane sample, its $\kappa(T)$ may include a considerable in-plane contribution.

We have further made a rough estimate of the mean free path l_p of heat-carrying phonons by employing the kinetic formula $\kappa = \frac{1}{3} C v_s l_p$. For phonon velocity we employ $v_s = 8300\ \text{m s}^{-1}$, which was obtained with first-principles calculations for the a axis [23]. Literature values of experimentally obtained specific heat $C(T)$ were used [36]. The calculated phonon mean free path $l_p(T)$ for in-plane thermal transport is shown in Fig. 4(b). The value of $l_p(T)$ is gradually enhanced with decreasing temperature, from 8 nm at RT to 2 μm at $T = 20$ K. However, the maximum value of l_p is still significantly smaller than the sample thickness, $\sim 100\ \mu$m, indicating that the values of $\kappa(T)$ are not restricted by sample size and the intrinsic thermal conductivity could be much higher. This is consistent with the inference drawn from the deviation of $\kappa(T)$ from the T^{-1} dependence.

C. Thermoelectric power and Nernst effect

The temperature-dependent thermoelectric power $S_{xx}(T)$ and Nernst coefficient $\nu(T)$ are shown in Figs. 5(a) and 5(b), respectively. $S_{xx}(T)$ of the in-plane samples reveals a relatively weak temperature dependence with largely enhanced values in the temperature range 50–200 K, i.e., the regime dominated by extrinsic charge carriers. The value of $S_{xx}(T)$ amounts to 480 μV/K at $T = 200$ K for sample IP1. It decreases drastically below $T = 50$ K, where both $\rho_{xx}(T)$ and $R_H(T)$ strongly increase with decreasing T, and above $T = 200$ K, too, where intrinsic charge transport was evidenced. For the through-plane sample, the aforementioned feature is largely weakened, and $S_{xx}(T)$ increases rather smoothly from $T = 2$ to 250 K.

The values of the Nernst coefficient $\nu(T)$ shown in Fig. 5(b) were estimated from the initial slope of $S_{xy}(B)$, i.e., $\nu = (\delta S_{xy}/\delta B)_{0T}$ [see Fig. 6(b) for the isotherms of $S_{xy}(B)$]. While the value of $\nu(T)$ is much smaller for IP2, its temperature profile is practically identical to that of IP1. A broad maximum of $\nu(T)$ appears again at the characteristic temperature

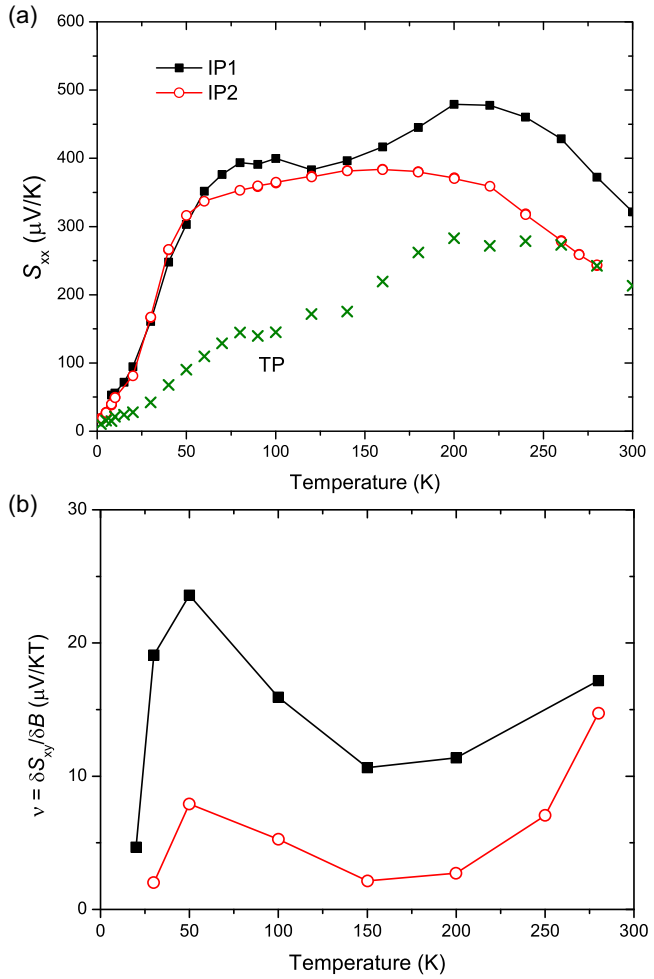

FIG. 5. (a) Thermoelectric power S_{xx} as a function of temperature measured for the two in-plane and one through-plane samples. (b) Nernst coefficient $\nu = \delta S_{xy}/\delta B$ of the two in-plane samples, estimated at zero-field limit.

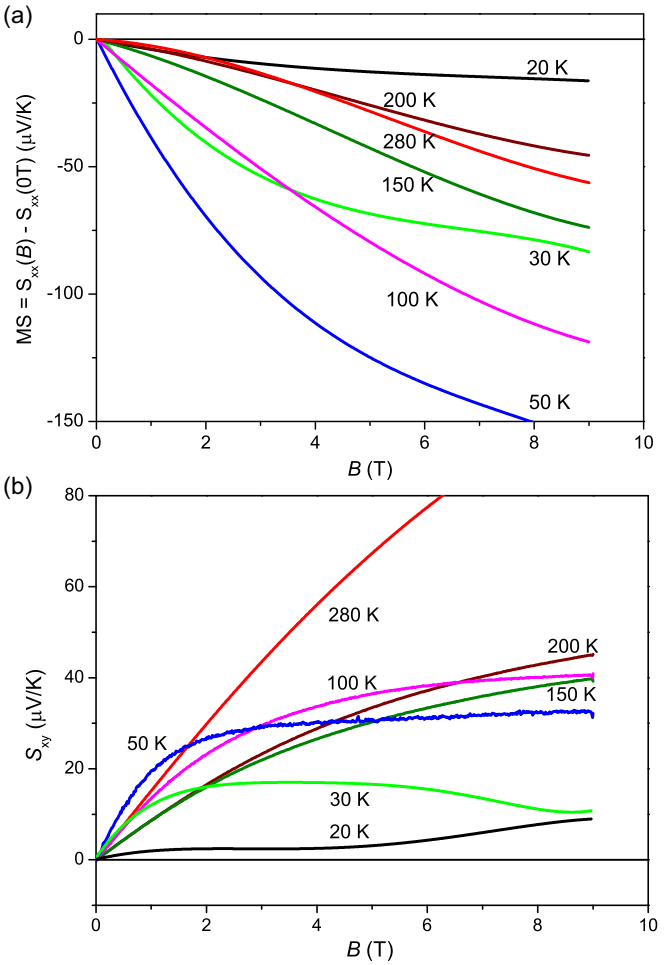

FIG. 6. (a) Magnetothermoelectric power, defined as MS $= S_{xx}(B) - S_{xx}(0T)$, as a function of magnetic field for the in-plane sample IP1. (b) Isothermal Nernst response S_{xy} as a function of field for the same sample.

$T \approx 50$ K, where extrinsic charge carriers at impurity levels start to get frozen out with decreasing temperature. Upon increasing temperature, $\nu(T)$ reveals a broad minimum at approximately 150 K, in contrast to the enhanced values of $S_{xx}(T)$ in the same temperature window. Most interestingly, at $T > 200$ K, $\nu(T)$ increases again despite the decrease of both $S_{xx}(T)$ and $\mu_{\rm H}(T)$ with temperature. The opposite trends in $S_{xx}(T)$ and $S_{xy}(T)$, as well as the intrinsic transport features observed in $\rho_{xx}(T)$, hint at an ambipolar transport at high temperatures, i.e., $T > 200$ K. There, both thermally activated electrons and holes significantly contribute to the electrical and thermoelectric transports. In this temperature range, while compensation caused by charge carriers with opposite signs diminishes S_{xx}, the Nernst effect can be largely enhanced because it measures the asymmetric relaxation time with respect to kinetic energy and is insensitive to the sign of charge carriers [37]. Indeed, an enhanced Nernst effect is a generic feature frequently seen in compensated semiconductors or semimetals, e.g., bismuth [38].

To gain further insight into the thermoelectric response related to the multiband effect, we show the magnetothermoelectric power defined as MS $= S_{xx}(B) - S_{xx}(0\,{\rm T})$ for IP1 as a function of field for various temperatures [see Fig. 6(a)]. At all temperatures above 10 K, MS(B) is negative, and its absolute value increases with field. Namely, $S_{xx}(B)$ decreases with increasing field. Such behavior is uncommon for a nonmagnetic semiconductor, where MS is, in general, expected to be positive, resembling MR (see discussion below), as is known for, e.g., germanium [39]. By contrast, the behavior of $S_{xy}(B)$ is typical of a semimetal or semiconductor [Fig. 6(b)]: it smoothly increases with field at $T > 50$ K and becomes a nonmonotonic function of field only at lower temperatures where $\mu_{\rm H}$ is high and $\mu_{\rm H}B \gg 1$ [40].

Recent thermoelectric measurements performed in a magnetic field on topological materials, such as $Pb_{1-x}Sn_xSe$ [40] and Cd_3As_2 [41], have shown strong field dependence of the thermoelectric properties due to the high-mobility Dirac fermions. A well-established approach to the field-dependent thermoelectric coefficients S_{ij} in these high-mobility materials is based on a matrix formulation of conductivity σ_{ij} [40]. By employing the two conductivity elements $\sigma_{xx} = \rho_{xx}/(\rho_{xx}^2 + \rho_{xy}^2)$ and $\sigma_{xy} = \rho_{xy}/(\rho_{xx}^2 + \rho_{xy}^2)$, the longitudinal and

transverse thermoelectric coefficients are expressed as

$$S_{xx}(B) = \frac{\pi^2}{3}\frac{k_B^2 T}{e}\left(\frac{\sigma_{xx}^2}{\sigma_{xx}^2+\sigma_{xy}^2}D + \frac{\sigma_{xy}^2}{\sigma_{xx}^2+\sigma_{xy}^2}D_H\right), \quad (1)$$

$$S_{xy}(B) = \frac{\pi^2}{3}\frac{k_B^2 T}{e}\frac{\sigma_{xx}\sigma_{xy}}{\sigma_{xx}^2+\sigma_{xy}^2}(D_H - D), \quad (2)$$

where $D = \partial \ln \sigma_{xx}/\partial\epsilon$ and $D_H = \partial \ln \sigma_{xy}/\partial\epsilon$ at the Fermi level ϵ_F. The complex variations of S_{xx} and S_{xy} as a function of field in high-mobility materials [40,41] can be ascribed to the competition between the diagonal and off-diagonal thermoelectric components, D and D_H. The sublinear enhancement of $S_{xy}(B)$ at $T > 100$ K as shown in Fig. 6(b) hints at a semiclassical transport behavior realized when $\sigma_{xy} \ll \sigma_{xx}$ [40]. There, Eqs. (1) and (2) reduce to the more familiar Mott formulas,

$$S_{xx}(B) = \frac{\pi^2}{3}\frac{k_B^2 T}{e}D, \quad (3)$$

$$S_{xy}(B) = \frac{\pi^2}{3}\frac{k_B^2 T}{e}\theta(D_H - D) = \frac{\pi^2}{3}\frac{k_B^2 T}{e}\frac{\partial\theta}{\partial\epsilon}\bigg|_{\epsilon=\epsilon_F}, \quad (4)$$

where $\theta = \sigma_{xy}/\sigma_{xx}$ is the Hall angle, which equals $\mu_H B$ in a one-band approximation.

A careful analysis of the above formulas, however, reveals a failure of their application to the negative MS(B) of BP. This is true at least in the semiclassical regime where $\sigma_{xy} \ll \sigma_{xx}$ (or, $\mu_H B \ll 1$). Assuming an unchanged $\partial\sigma_{xx}/\partial\epsilon$ in moderate magnetic field for a given electronic structure, it is straightforward that a decrease in electrical conductivity σ_{xx} (namely, positive MR) will lead to an increase in $\partial \ln \sigma_{xx}/\partial\epsilon$; then the absolute value of S_{xx} increases. The assumption of an unchanged $\partial\sigma_{xx}/\partial\epsilon$ is reasonable for most nonmagnetic semiconductors like BP, where the energy derivative of σ_{xx} at ϵ_F is determined by an energy-dependent electronic density of states. To interpret the negative MS(B) as shown in Fig. 6(a), a feasible approach is to consider an ambipolar contribution from both hole- and electronlike charge carriers. An increasing contribution from the latter upon increasing field can naturally lead to negative MS(B); that is, S_{xx} decreases with B. This is consistent with the inference drawn from the T-dependent thermoelectric power and Nernst coefficient at $T > 200$ K (see Fig. 5). The failure of Eqs. (1) and (2) in the ambipolar transport regime has already been suggested [40].

The potential application of BP as a thermoelectric material has been intensively discussed from a theoretical point of view [15,16,18,42]. To make an experimental assessment, in Fig. 7 we show the thermoelectric power factor, PF $= S_{xx}^2/\rho_{xx}$, as a function of temperature for sample IP1. The obtained values of PF(T) fall between 0.1 and 0.4 μW K^{-2} cm^{-1} in a large temperature range from $T = 30$ K to RT, which is more than two orders of magnitude smaller than the state-of-the-art thermoelectrics. Actually, pristine BP as investigated in this work has a carrier concentration of $\sim 10^{16}$ cm^{-3} or even less [Fig. 3(b), inset], four orders of magnitude smaller than the theoretically predicted carrier concentration for maximum thermoelectric performance [16,42]. This guarantees a large parameter space for further thermoelectric optimization towards a large PF, i.e., an enhanced electrical conductivity and, meanwhile, a diminished ambipolar thermoelectric effect. As has been theoretically shown, an appropriate mechanical strain [15,42] or chemical substitution by, e.g., Sb can indeed enhance the thermoelectric power factor greatly [16].

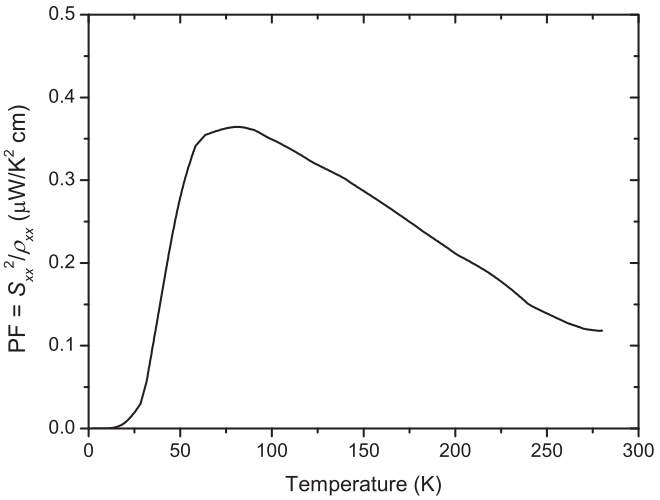

FIG. 7. Thermoelectric power factor, PF $= S_{xx}^2/\rho_{xx}$, as a function of temperature for the in-plane sample IP1.

IV. SUMMARY AND CONCLUSION

Our combined thermal, electrical, and thermoelectric measurements on bulk single-crystalline BP reveal consistent transport evidence that pristine undoped BP is a p-type semiconductor with dominant transport of extrinsic charge carriers in a substantial range below $T \approx 200$ K. In order to interpret the temperature- and field-dependent electrical and thermoelectric properties consistently, we propose the importance of ambipolar transport with different types of charge carriers. A high in-plane thermal conductivity maximum of $\kappa = 180$ W/m K at $T \approx 25$ K has been observed. This value, however, is still largely constrained by other extrinsic phonon scattering events, probably due to, e.g., charge carriers. Therefore, in a pure enough BP with high crystallinity, to what extent the in-plane thermal conductivity can be enhanced has yet to be clarified for potential applications as nanoelectronics and optoelectronics. However, as far as the thermoelectric properties are concerned, the aforementioned two outstanding features of bulk BP, i.e., the ambipolar transport and the high lattice thermal conductivity, will degrade the performance significantly. Both chemical doping and external electric field are frequently employed to change the chemical potential of a semiconductor. These yield the most effective way to modulate the electron-hole asymmetry for better thermoelectricity and the number of charge carriers for high electrical conduction. The latter will serve as phonon scatterers as well. Indeed, enhanced thermoelectric power has been observed in nanoscaled BP devices with application of appropriate gate voltage [43,44]. Furthermore, the ambipolar conduction, as well as the band gap E_g, is tunable through layer thickness [4]. How thermoelectric properties evolve with layer thickness seems intriguing as well.

To conclude, by investigating a rather complete set of electrical and thermal transport coefficients, we found that pristine bulk single-crystalline BP is largely influenced by extrinsic charge carriers below room temperature, with significant ambipolar transport due to opposite types of charge carriers. While the observed in-plane thermal conductivity is among the largest values so far reported for BP, it is still largely constrained by extrinsic phonon scatterers such as charge carriers. Therefore, the electronic, thermal, and thermoelectric properties are still far from being optimized for various potential applications. Further investigation of the transport properties of bulk BP by shifting the chemical potential in a well-controlled way appears to be of great interest.

ACKNOWLEDGMENTS

This work was supported by the National Science Foundation of China (Grant No. 11474332), MOST of China (Grants No. 2015CB921303 and No. 2017YFA0206303), and the Chinese Academy of Sciences through the strategic priority research program (XDB07020200).

[1] X. Ling, H. Wang, S. Huang, F. Xia, and M. S. Dresselhaus, Proc. Natl. Acad. Sci. U.S.A. **112**, 4523 (2015).
[2] H. Liu, A. T. Neal, Z. Zhu, Z. Luo, X. Xu, D. Tomanek, and P. D. Ye, ACS Nano **8**, 4033 (2014).
[3] A. K. Geim and S. K. Novoselov, Nat. Mater. **6**, 183 (2007).
[4] S. Das, W. Zhang, M. Demarteau, A. Hoffmann, M. Dubey, and A. Roelofs, Nano Lett. **14**, 5733 (2014).
[5] H. Asahina, K. Shindo, and K. Morita, J. Phys. Soc. Jpn. **51**, 1193 (1982).
[6] J. Qiao, X. Kong, Z.-X. Hu, F. Yang, and W. Ji, Nat. Commun. **5**, 4475 (2014).
[7] A. Jain and A. J. H. McGaughey, Sci. Rep. **5**, 8501 (2015).
[8] J. W. Jiang, Nanotechnology **26**, 055701 (2015).
[9] L. Li, F. Yang, G. J. Ye, Z. Zhang, Z. Zhu, W. Lou, X. Zhou, L. Li, K. Watanabe, T. Taniguchi, K. Chang, Y. Wang, X. H. Chen, and Y. Zhang, Nat. Nanotechnol. **11**, 593 (2016).
[10] X. Chen, Y. Wu, Z. Wu, Y. Han, S. Xu, L. Wang, W. Ye, T. Han, Y. He, Y. Cai, and N. Wang, Nat. Commun. **6**, 7315 (2015).
[11] Z. J. Xiang, G. J. Ye, C. Shang, B. Lei, N. Z. Wang, K. S. Yang, D. Y. Liu, F. B. Meng, X. G. Luo, L. J. Zou, Z. Sun, Y. Zhang, and X. H. Chen, Phys. Rev. Lett. **115**, 186403 (2015).
[12] C. H. Li, Y. J. Long, L. X. Zhao, L. Shan, Z. A. Ren, J. Z. Zhao, H. M. Weng, X. Dai, Z. Fang, C. Ren, and G. F. Chen, Phys. Rev. B **95**, 125417 (2017).
[13] M. Karuzawa, M. Ishizuka, and S. Endo, J. Phys. Condens. Matter **14**, 10759 (2002).
[14] G. A. Slack, Phys. Rev. **139**, A507 (1965).
[15] G. Qin, Q. B. Yan, Z. Qin, S. Y. Yue, H. J. Gui, Q. R. Zheng, and G. Su, Sci. Rep. **4**, 6946 (2014).
[16] J. Zhang, H. J. Liu, L. Cheng, J. Wei, J. H. Liang, D. D. Fan, P. H. Jiang, L. Sun, and J. Shi, J. Mater. Chem. C **4**, 991 (2016).
[17] L. D. Zhao, S. H. Lo, Y. Zhang, H. Sun, G. Tan, C. Uher, C. Wolverton, V. P. Dravid, and M. G. Kanatzidis, Nature (London) **508**, 373 (2014).
[18] R. Fei, A. Faghaninia, R. Soklaski, J. A. Yan, C. Lo, and L. Yang, Nano Lett. **14**, 6393 (2014).
[19] E. Flores, J. R. Ares, A. Castellanos-Gomez, M. Barawi, I. J. Ferrer, and C. Sánchez, Appl. Phys. Lett. **106**, 022102 (2015).
[20] Y. Wang, G. Xu, Z. Hou, B. Yang, X. Zhang, E. Liu, X. Xi, Z. Liu, Z. Zeng, W. Wang, and G. Wu, Appl. Phys. Lett. **108**, 092102 (2016).
[21] Z. Hou, B. Yang, Y. Wang, B. Ding, X. Zhang, Y. Yao, E. Liu, X. Xi, G. Wu, Z. Zeng, Z. Liu, and W. Wang, Sci. Rep. **6**, 23807 (2016).
[22] J. Zhu, H. Park, J. Y. Chen, X. Gu, H. Zhang, S. Karthikeyan, N. Wendel, S. A. Campbell, M. Dawber, X. Du, M. Li, J. P. Wang, R. Yang, and X. Wang, Adv. Electron. Mater. **2**, 1600040 (2016).
[23] B. Sun, X. Gu, Q. Zeng, X. Huang, Y. Yan, Z. Liu, R. Yang, and Y. K. Koh, Adv. Mater. **29**, 1603297 (2016).
[24] H. Jang, J. D. Wood, C. R. Ryder, M. C. Hersam, and D. G. Cahill, Adv. Mater. **27**, 8017 (2015).
[25] Y. Akahama, S. Endo, and S. Narita, J. Phys. Soc. Jpn. **52**, 2148 (1983).
[26] Y. Akahama and H. Kawamura, Phys. Status Solidi B **223**, 349 (2001).
[27] K. Akiba, A. Miyake, Y. Akahama, K. Matsubayashi, Y. Uwatoko, and M. Tokunaga, Phys. Rev. B **95**, 115126 (2017).
[28] R. W. Keyes, Phys. Rev. **92**, 580 (1953).
[29] M. Baba, F. Izumida, Y. Takeda, K. Shibata, A. Morita, Y. Koike, and T. Fukase, J. Phys. Soc. Jpn. **60**, 3777 (1991).
[30] Y. Akahama and S. Endo, Solid State Commun. **104**, 307 (1997).
[31] Z. Luo, J. Maassen, Y. Deng, Y. Du, R. P. Garrelts, M. S. Lundstrom, P. D. Ye, and X. Xu, Nat. Commun. **6**, 8572 (2015).
[32] S. Lee, F. Yang, J. Suh, S. Yang, Y. Lee, G. Li, H. S. Choe, A. Suslu, Y. Chen, C. Ko, J. Park, K. Liu, J. Li, K. Hippalgaonkar, J. J. Urban, S. Tongay, and J. Wu, Nat. Commun. **6**, 8573 (2015).
[33] L. Zhu, G. Zhang, and B. Li, Phys. Rev. B **90**, 214302 (2014).
[34] A. A. Balandin, Nat. Mater. **10**, 569 (2011).
[35] J. C. Thompson and B. A. Younglove, J. Phys. Chem. Solids **20**, 146 (1961).
[36] M. Yoshizawa, I. Shirotani, and T. Fujimura, J. Phys. Soc. Jpn. **55**, 1196 (1986).
[37] P. Sun, B. Wei, D. Menzel, and F. Steglich, Phys. Rev. B **90**, 245146 (2014).
[38] K. Behnia, J. Phys. Condens. Matter **21**, 113101 (2009).
[39] M. C. Steele, Phys. Rev. **107**, 81 (1957).
[40] T. Liang, Q. Gibson, J. Xiong, M. Hirschberger, S. P. Koduvayur, R. J. Cava, and N. P. Ong, Nat. Commun. **4**, 2696 (2013).
[41] Z. Jia, C. Li, X. Li, J. Shi, Z. Liao, D. Yu, and X. Wu, Nat. Commun. **7**, 13013 (2016).
[42] H. Y. Lv, W. J. Lu, D. F. Shao, and Y. P. Sun, Phys. Rev. B **90**, 085433 (2014).
[43] S. J. Choi, B. K. Kim, T. H. Lee, Y. H. Kim, Z. Li, E. Pop, J. J. Kim, J. H. Song, and M. H. Bae, Nano Lett. **16**, 3969 (2016).
[44] Y. Saito, T. Iizuka, T. Koretsune, R. Arita, S. Shimizu, and Y. Iwasa, Nano Lett. **16**, 4819 (2016).